Journal of Alloys and Compounds 509 (2011) 3382–3386

Contents lists available at ScienceDirect

Journal of Alloys and Compounds

journal homepage: www.elsevier.com/locate/jallcom

Investigation of the thermal and magnetic properties of $Fe_{61}Co_{10}Zr_2$ $Fe_{61}Co_{10}Zr_{2.5}Hf_{2.5}Me_2W_2B_{20}$ (Me = Y, Nb, W, Ti, Mo, Ni) bulk amorphous alloys obtained by an induction suction method

Marcin G. Nabiałek[a], Marcin J. Dośpiał[a,*], Michał Szota[b], Pawel Pietrusiewicz[a], Jarosław Jędryka[b]

[a] Institute of Physics, Częstochowa University of Technology, 19 Armii Krajowej Av., 42-200 Częstochowa, Poland
[b] Institute of Materials Engineering, Częstochowa University of Technology, 19 Armii Krajowej Av., 42-200 Częstochowa, Poland

ARTICLE INFO

Article history:
Received 29 June 2010
Received in revised form 6 December 2010
Accepted 13 December 2010
Available online 21 December 2010

PACS:
75.50.Bb
75.50.Kj
65.60+a
75.60 Ej
76.80.+y
61.05.C
61.05.Qr

Keywords:
Fe and its alloys
Amorphous magnetic materials
Thermal properties of amorphous solids and glasses
Magnetization curves
Hysteresis
Mössbauer effect
X-ray diffraction
Mössbauer spectroscopy

ABSTRACT

The microstructure, magnetic properties and thermal stability of $Fe_{61}Co_{10}Zr_{2.5}Hf_{2.5}Me_2W_2B_{20}$ (Me = Y, Nb, W, Ti, Mo, Ni) alloys were investigated. The samples were obtained by an induction suction method as 0.5 mm thickness plates. The microstructure was examined using X-ray diffraction and Mössbauer spectroscopy. It was shown that the investigated samples have amorphous structure throughout the volumes of the samples. The magnetic properties were measured using a Vibrating Sample Magnetometer. The investigated alloys are soft magnetic materials with low coercivity field (from 5.8 A/m to 54 A/m) and high saturation of the magnetization (from 0.87 T to 1.26 T). The studies of thermal stability were performed using a differential scanning calorimeter. It was shown that the addition of respective atoms led to changes of Curie temperature in the range from 497 to 587 K, depending on the composition of the alloys.

1. Introduction

In recent years large quantity of data has been published about production methods of bulk metallic glasses (BMG). The most popular methods are suction casting [1,2] and injection casting [3]. These methods are (respectively) based on suction or injection of a liquid alloy onto a water-cooled copper mould. The cooling speed in comparison to the classical melt-spinning method is much slower, what significantly limits the production possibilities for BMGs.

A great breakthrough in requirements for the alloy compositions was made by Inoue, in 1989 [4]. He showed that significant improvement of glass forming ability (GFA) can be achieved by production of a multicomponent alloy with the addition of large atoms (atomic radius 12% larger or smaller than the radius of base atoms) and negative mixing heat among the basic components.

The first BMGs based on iron were produced in 1995 from mixtures of Fe–(Nb, Mo)–(Al, Ga)–(P,C, B, Si, Ge) [5]. The bulk metallic glasses based on iron or cobalt display good mechanical (high toughness, large density) and soft magnetic properties (high value of initial permeability, low coercivity field and high magnetization saturation) [6,7]. These features led to a wide range of applications for these materials.

$Fe_{61}Co_{10}Zr_{2.5}Hf_{2.5}Me_2W_2B_{20}$ (where Me = Y, Nb, W, Ti, Mo, Ni) amorphous alloys are an interesting group of materials. The paper discusses one method of their production as well as their microstructure and magnetic properties. These materials properties mostly depend on Me addition [8–21]. The appropriate composition, allow to produce soft ferromagnetic material with

* Corresponding author. Tel.: +48 34 3250610; fax: +48 34 3250795.
E-mail address: mdospial@wp.pl (M.J. Dośpiał).

0925-8388/$ – see front matter © 2010 Elsevier B.V. All rights reserved.
doi:10.1016/j.jallcom.2010.12.075

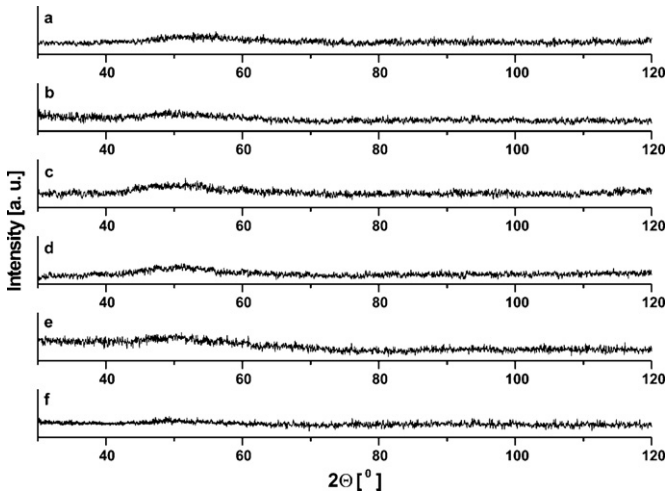

Fig. 1. X-ray diffraction patterns of (a) $Fe_{61}Co_{10}Zr_{2.5}Hf_{2.5}Ni_2W_2B_{20}$, (b) $Fe_{61}Co_{10}Zr_{2.5}Hf_{2.5}Nb_2W_2B_{20}$, (c) $Fe_{61}Co_{10}Zr_{2.5}Hf_{2.5}Y_2W_2B_{20}$, (d) $Fe_{61}Co_{10}Zr_{2.5}Hf_{2.5}Ti_2W_2B_{20}$, (e) $Fe_{61}Co_{10}Zr_{2.5}Hf_{2.5}Mo_2$ W_2B_{20}, and (f) $Fe_{61}Co_{10}Zr_{2.5}Hf_{2.5}W_4B_{20}$ alloys in the as-quenched state.

low coercivity and the relatively high saturation of the magnetization. Most of these alloys are also characterized by good functional properties: high microhardness, corrosion resistance, wide range of extent of the supercooled liquid region and good thermal stability.

In this work, the microstructure, thermal stability and magnetic properties of $Fe_{61}Co_{10}Zr_{2.5}Hf_{2.5}Me_{4-x}W_2B_{20}$ (Me = Nb, Mo, Ti, Y, Ni) bulk amorphous alloys were investigated.

2. Experimental procedure

The bulk amorphous $Fe_{61}Co_{10}Zr_{2.5}Hf_{2.5}Me_{4-x}W_2B_{20}$ (Me = Nb, Mo, Ti, Y, Ni) alloys were obtained by suction of the liquid alloy onto a water-cooled copper mould (induction suction method). In order to obtain homogenous material, the ingots were repeatedly arc-remelted under argon atmosphere in the presence of an oxygen absorber (liquid, pure Ti). Ingots of the desired alloys were prepared using high purity elements (Fe, Co, Zr, Hf, Ti, W, Nb, Ni, Mo, Y of over 99.99% purity). Addition of boron was performed using an alloy with purity above 99.99% with well-known composition ($Fe_{45.6}B_{54.4}$). The samples were produced as plates with 0.5 mm thickness and 1 cm^2 area.

The structure of the as cast samples have been investigated using X-ray diffraction (XRD) and the Mössbauer spectroscopy. The X-ray diffraction patterns were taken using cobalt source with a moderate wavelength of 1.79021 Å, exposure time 10 s and step angle 0.02°. The Mössbauer spectra were recorded using a conventional POLON spectrometer with constant-acceleration and the ^{57}Co of γ-ray source in a rhodium matrix with half-life time of 273 days. The spectrometer was calibrated using Fe foil. The alloys for X-ray diffraction and Mössbauer spectroscopy were ground into powder.

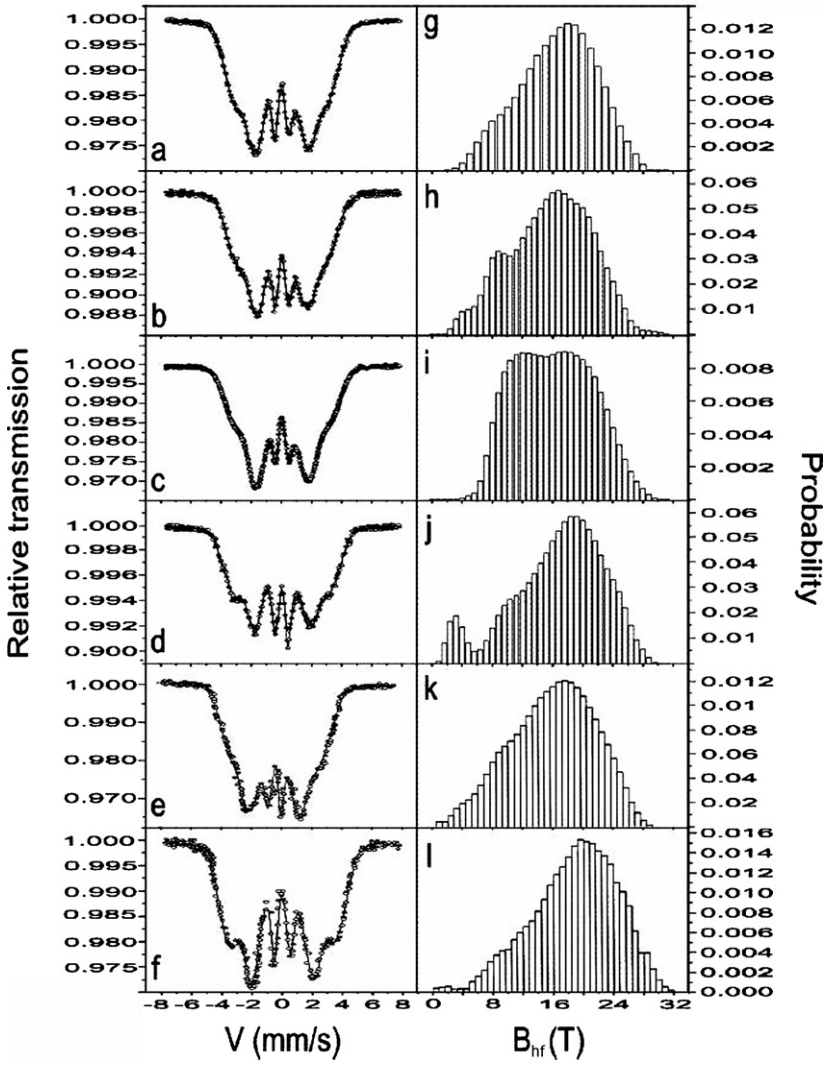

Fig. 2. Transmission Mössbauer spectra and corresponding hyperfine field distributions of the $Fe_{61}Co_{10}Zr_{2.5}Hf_{2.5}Me_xW_{4-x}B_{20}$ alloys in the as-quenched state where (a and g) Me = Y, $x = 2$; (b and h) Me = Nb, $x = 2$; (c and i) $x = 0$; (d and j) Me = Ti, $x = 2$; (e and k) Me = Mo, $x = 2$; and (f and l) Me = Ni, $x = 2$.

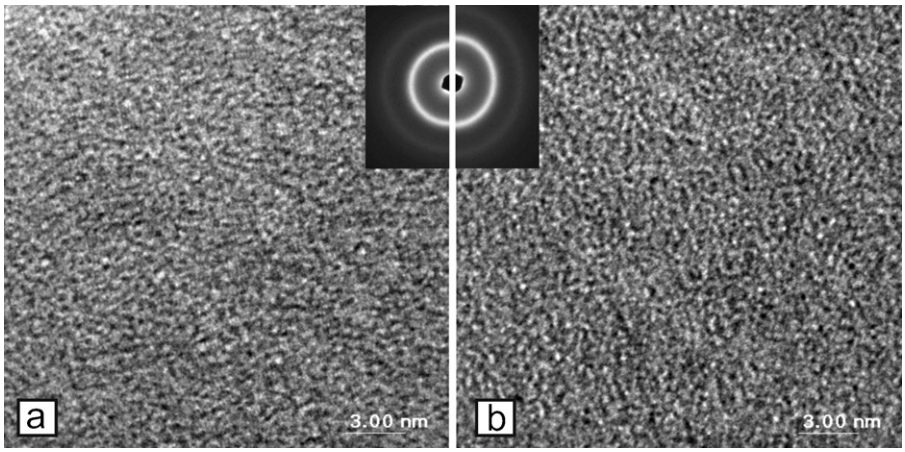

Fig. 3. Exemplary high resolution TEM images of the structure and the corresponding electronograms (inset) for (a) $Fe_{61}Co_{10}Zr_{2.5}Hf_{2.5}Nb_2W_2B_{20}$ and $Fe_{61}Co_{10}Zr_{2.5}Hf_{2.5}Ti_2W_2B_{20}$ (b) amorphous alloy in the as-quenched state.

The observations of microstructure were also carried out by using the high resolution transmission electron microscopy (HRTEM) JEOL 3010. The samples for microstructure observation were first polished using emery paper and diamond pastes of the gradation from 2 to 0.5 μm with an ethanol as a water free lubricant and ion thinned in a GATAN Ion Mill.

The magnetic properties (the coercivity H_C, the remanence $\mu_0 M_R$ and the saturation of the magnetization M_S) were measured using a LakeShore VSM magnetometer of maximum field of 2 T. The Curie temperatures for the all investigated samples were derived from thermomagnetic curves obtained using a force magnetometer.

Thermal stability of the investigated alloys was obtained using a differential scanning calorimeter (DSC) with a constant heating rate of 10 K/min. From the DSC plots several characteristic temperatures including: the glass transition temperature (T_g), the crystallization temperature (T_x), extent of the supercooled liquid region (ΔT_x), the primary crystallization temperature (T_1), the secondary crystallization temperature (T_2), undercooled temperature (ΔT_l), the melting temperature (T_m), the liquidus temperature (T_l) [22]. These data were also used to derive several other parameters: $\Delta T_m = T_l - T_m$ interval temperature, $\Delta T_x = T_x - T_g$ extent of the supercooled liquid region, $\Delta T_l = T_l - T_x$ undercooled temperature, $T_{rg} = T_g/T_m$ [23] reduced glass transition temperature, $\gamma_m = (2T_x - T_g)/T_l$ modified GFA parameter, $\gamma = T_x/(T_g + T_x)$ [24–26] relative GFA parameter and $\delta = T_x/(T_l + T_g)$ [27].

3. Results and discussion

For all measured samples, XRD patterns are similar (Fig. 1). The deficiency of distinct, narrow peaks suggests a lack of crystalline phase. The presence of wide, diffused maxima around 2θ angle of 51° is typical for bulk amorphous alloys based on iron.

The Mössbauer spectra were used to confirm the amorphous structure of the sample on the basis of previously performed X-ray diffraction measurements. The Mössbauer spectra for all the measured samples were asymmetric and consisted of wide, overlapping lines (Fig. 2a–f) typical for amorphous ferromagnets. Usually the first crystalline phase which appears in the Fe–Co based alloys, during production process is α-Fe. The hyperfine field induction for this phase is about 34 T, additionally it is not characterized by a broad distribution but only a single line (or very narrow distribution). In the case of the presented spectra it was not possible to fit additional sextet corresponding to the crystalline phase.

Table 1
The average hyperfine induction $(B_{eff})_{am}$, its standard deviation D_{am} measured for all investigated samples.

Alloy composition	$(B_{eff})_{am}$ (T)	D_{am} (T)
$Fe_{61}Co_{10}Zr_{2.5}Hf_{2.5}Y_2W_2B_{20}$	17.53	5.08
$Fe_{61}Co_{10}Zr_{2.5}Hf_{2.5}Nb_2W_2B_{20}$	15.70	5.35
$Fe_{61}Co_{10}Zr_{2.5}Hf_{2.5}W_4B_{20}$	16.75	6.01
$Fe_{61}Co_{10}Zr_{2.5}Hf_{2.5}Ti_2W_2B_{20}$	15.52	5.08
$Fe_{61}Co_{10}Zr_{2.5}Hf_{2.5}Mo_2W_2B_{20}$	15.71	5.09
$Fe_{61}Co_{10}Zr_{2.5}Hf_{2.5}Ni_2W_2B_{20}$	19.91	5.11

Table 2
The magnetic parameters and Curie temperatures measured for all investigated samples.

Alloy composition	H_C (A/m)	M_S (T)	T_C (K)
$Fe_{61}Co_{10}Zr_{2.}5Hf_{2.5}Y_2W_2B_{20}$	26.4	1.12	509
$Fe_{61}Co_{10}Zr_{2.5}Hf_{2.5}Nb_2W_2B_{20}$	22	1.06	499
$Fe_{61}Co_{10}Zr_{2.5}Hf_{2.5}W_4B_{20}$	33.5	1.14	497
$Fe_{61}Co_{10}Zr_{2.5}Hf_{2.5}Ti_2W_2B_{20}$	54	0.87	510
$Fe_{61}Co_{10}Zr_{2.5}Hf_{2.5}Mo_2W_2B_{20}$	5.8	1.05	515
$Fe_{61}Co_{10}Zr_{2.5}Hf_{2.5}Ni_2W_2B_{20}$	10.3	1.26	587

From hyperfine magnetic field distributions on Fe sites, it was also deduced that the most homogenous iron distribution in the volume of the sample was observed for $Fe_{61}Co_{10}Zr_{2.5}Hf_{2.5}Y_2W_2B_{20}$ (Fig. 2g) and $Fe_{61}Co_{10}Zr_{2.5}Hf_{2.5}Mo_2W_2B_{20}$ (Fig. 2k) alloys.

For all of the remaining samples, additional components in the hyperfine field distribution were observed. The presence of at least two components suggests regions with different iron concentration and results from heterogeneous iron distribution in the volume of the samples. The average hyperfine induction $(B_{eff})_{am}$ and its standard deviation D_{am} are presented in Table 1.

Fig. 3 presents exemplary high resolution TEM pictures of structure and the corresponding electronograms (inset) made for $Fe_{61}Co_{10}Zr_{2.5}Hf_{2.5}Ni_2W_2B_{20}$ and $Fe_{61}Co_{10}Zr_{2.5}Hf_{2.5}Ti_2W_2B_{20}$ amorphous alloys in the as-quenched state. On the presented images it is not possible to distinguish an areas with periodic arrangement of atoms. The lack of a point reflections and presence of broad diffuse rings on electronograms from these areas also confirm amorphous structure of investigated materials.

From magnetic measurements it was found that all investigated alloys are soft ferromagnetic materials with low coercivity field (H_C) and high magnetization saturation (M_S). Figs. 4 and 5 show deviation of both parameters as a function of alloy composition.

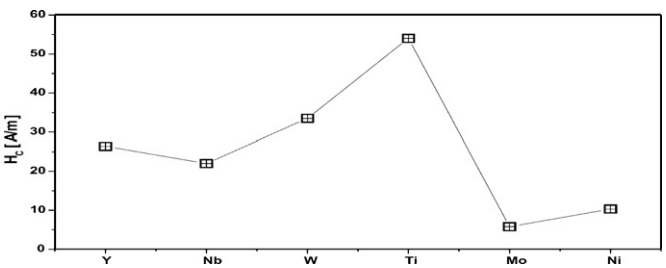

Fig. 4. The dependence of coercivity field as a function of alloy composition in the as-quenched state.

Table 3
The thermodynamics and GFA parameters measured for all investigated samples.

Alloy composition	T_g (K)	T_x (K)	T_m (K)	T_l (K)	ΔT_m (K)	ΔT (K)	ΔT_X (K)	T_{rg} (K)	γ_m	γ	δ
$Fe_{61}Co_{10}Zr_{2.5}Hf_{2.5}Y_2W_2B_{20}$	792	872	1336	1462	126	590	80	0.59	0.65	0.38	1.30
$Fe_{61}Co_{10}Zr_{2.5}Hf_{2.5}Nb_2W_2B_{20}$	788	885	1303	1450	147	565	97	0.60	0.67	0.39	1.33
$Fe_{61}Co_{10}Zr_{2.5}Hf_{2.5}W_4B_{20}$	813	871	1367	1493	126	680	58	0.59	0.62	0.35	1.31
$Fe_{61}Co_{10}Zr_{2.5}Hf_{2.5}Ti_2W_2B_{20}$	794	859	1331	1488	157	694	65	0.59	0.62	0.37	1.24
$Fe_{61}Co_{10}Zr_{2.5}Hf_{2.5}Mo_2W_2B_{20}$	790	838	1312	1462	150	624	48	0.60	0.60	0.37	1.24
$Fe_{61}Co_{10}Zr_{2.5}Hf_{2.5}Ni_2W_2B$	771	840	1316	1494	178	654	69	0.58	0.60	0.37	1.16

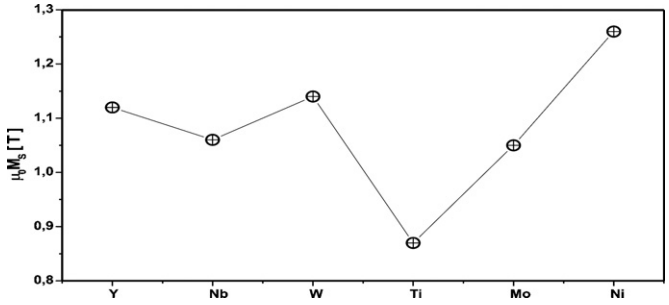

Fig. 5. The dependence of magnetization saturation as a function of alloy composition in the as-quenched state.

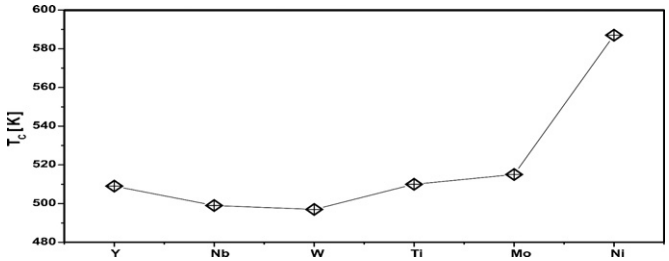

Fig. 6. Saturation of the polarization curves as a function of applied temperature and corresponding temperature dependencies of saturation of the polarization in $1/\beta$ power (inset) for all investigated alloys in the as-quenched state.

The thermomagnetic curves $\mu_0 M_S(T)$ were measured using a force magnetometer. The relation $[\mu_0 M_S(T)]^{(1/\beta)}$ (where $\beta = 0.36$ is the critical exponent in equation $\mu_0 M_S = \mu_0 M_0 \times (1 - T/T_C)^{\beta}$) was used to derive Curie temperature (T_C) for the Heisenberg ferromagnet (Fig. 6) [28]. All magnetic parameters are presented in Table 2.

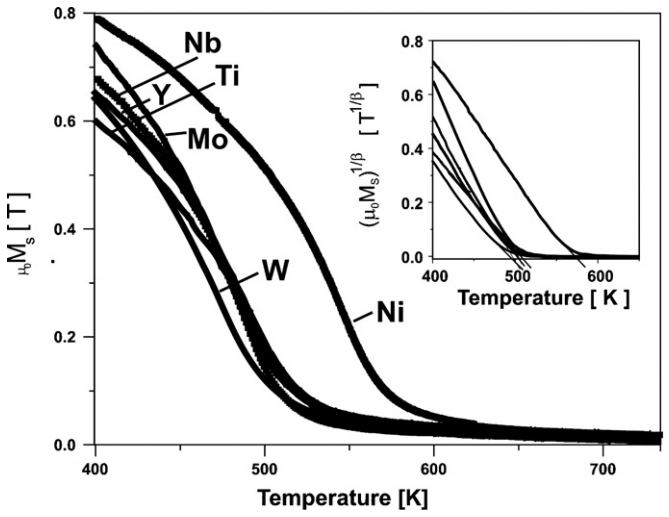

Fig. 7. The dependence of Curie temperature as a function of alloy composition in the as-quenched state.

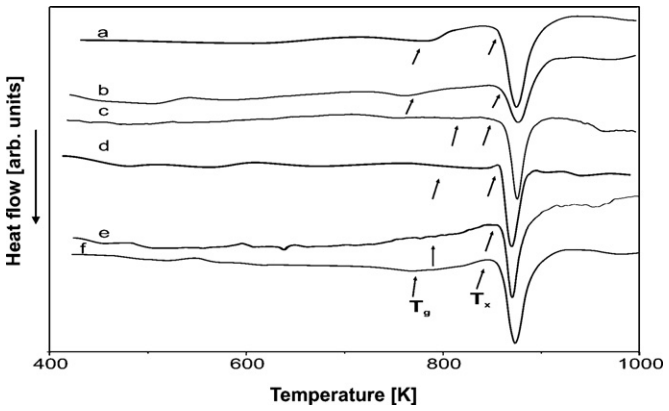

Fig. 8. DSC plots measured with constant temperature step in the range from 400 to 1000 K for as-quenched $Fe_{61}Co_{10}Zr_{2.5}Hf_{2.5}Me_xW_{4-x}B_{20}$ alloy Me = Y (a), Nb (b), W (c), Ti (d), Mo (e) and Ni (f).

For all measured samples, $Fe_{61}Co_{10}Zr_{2.5}Hf_{2.5}Mo_2W_2B_{20}$, $Fe_{61}Co_{10}Zr_{2.5}Hf_{2.5}Ni_2W_2B_{20}$ displayed the best soft magnetic properties, respectively: coercivity $H_C = 8$ or 10 A/m and saturation of the magnetization $M_S = 1$ or 1.25 T. Both samples also had good thermal stability of ferromagnetic state, resulting from high Curie temperatures $T_C = 515$ K for Mo and $T_C = 587$ K for Ni addition (Fig. 7).

The DSC plots presented in Fig. 8 were used to obtain characteristic temperatures. All these parameters were used to determine thermal stability of the investigated alloys and are listed in Table 3.

All investigated alloys displayed high values of reduced glass transition temperature, modified and relative GFA parameters as well as δ parameter resulting from good glass-forming ability. The best glass formability was displayed by alloys with Nb or Y addition what result from highest values of parameters like, respectively $T_{rg} = 0.60$ and 0.59, $\gamma_m = 0.67$ and 0.65, $\gamma = 0.39$ and 0.38 or $\delta = 1.33$ and 1.30. The ΔT_x parameter for these alloys indicates that supercooled liquid can exist in a broad temperature range 97 (for Nb) and 80 K (for Y addition) without crystallization.

4. Conclusions

The X-ray diffractometry and Mössbauer spectroscopy showed that suction-casting method allow to obtain bulk samples in the form of plates with fully amorphous structure.

Studies of the influence of selected alloying elements (Me = Y, Nb, W, Ti, Mo and Ni) on the glass formation ability, thermal stability and magnetic properties of $Fe_{61}Co_{10}Zr_{2.5}Hf_{2.5}Me_2W_2B_{20}$ amorphous alloys were performed.

For alloys where 2% of W was substituted by Y or Nb the highest crystallization temperature and the widest range of the supercooled liquid region were observed. The extend of supercooled liquid region for these alloys was equal respectively 80 K and 97 K, what was about 30 K higher then in the remaining alloys. These results show that the Nb and Y significantly improve the glass formation ability and delay the crystallization process of Fe–Co–Me–B type amorphous alloys. In turn, replacing of non-ferromagnetic W

on the ferromagnetic Ni raises the saturation of the magnetization for even a few tenths of Tesla's and the Curie temperature by tens of K in comparison to the remaining alloys. The magnetic interactions between Fe and Co atoms are weakened by additions of nonferromagnetic elements Me = Ti, Nb, Mo, Y, W.

$Fe_{61}Co_{10}Zr_{2.5}Hf_{2.5}Me_2W_2B_{20}$ (Me = Ti, Nb, Ni, Mo, Y, W) alloys due to the fairly good electrical characteristics may in future be used as a soft-ferromagnetic parts of transformer cores and medium power reactors operating at elevated temperatures and hard environmental conditions.

References

[1] A. Inoue, Z. Tao, Mater. Trans. Jpn. Inst. Met. 36 (1995) 1184–1187.
[2] Ch. Ma, N. Nishiyama, A. Inoue, Mater. Sci. Eng. A 407 (2005) 201–206.
[3] E.S. Park, D.H. Kim, J. Mater. Res. 19 (2004) 685–688.
[4] A. Inoue, N. Yano, T. Masumoto, J. Mater. Sci. 19 (1984) 279–306.
[5] A. Inoue, Acta Mater. 48 (2000) 279–306.
[6] M. Lubas, J. Zbroszczyk, M. Nabialek, J. Olszewski, K. Sobczyk, W. Ciurzyriska, M. Szota, P. Bragiel, J.P. Jasiriski, J. Świerczek, Arch. Metall. Mater. 53 (3) (2008).
[7] A. Inoue, T. Zhang, T. Masumoto, Mater. Trans. Jpn. Inst. Mater. 31 (1990) 177–183.
[8] A. Inoue, J.S. Gook, Mater. Trans. Jpn. Inst. Mater. 36 (1995) 1282.
[9] A. Inoue, J.S. Gook, Mater. Trans. Jpn. Inst. Mater. 37 (1996) 32.
[10] L.B. Shen, H. Koshiba, H. Kimura, A. Inoue, M. Omori, A. Okubo, Mater. Trans. Jpn. Inst. Mater. 43 (2002) 1961.
[11] B.L. Shen, A. Inoue, Mater. Trans. Jpn. Inst. Mater. 43 (2002) 1235.
[12] B.L. Shen, H. Koshiba, H. Kimura, A. Inoue, T. Mizushima, Mater. Trans. Jpn. Inst. Mater. 41 (2002) 1675.
[13] B.L. Shen, H. Koshiba, H. Kimura, A. Inoue, Mater. Trans. Jpn. Inst. Mater. 41 (2000) 1478.
[14] H. Chiriac, N. Lupu, J. Magn. Magn. Mater. 215 (2000) 394.
[15] H. Chiriac, N. Lupu, Physica B 299 (2001) 293.
[16] W. Zhang, A. Inoue, Mater. Trans. 42 (2001) 1142.
[17] W. Zhang, A. Inoue, Mater. Trans. 42 (2001) 1835.
[18] W. Zhang, M. Matsuhide, C. Li, H. Kimura, A. Inoue, Mater. Trans. 42 (2001) 2059.
[19] F. Li, T. Zhang, A. Inoue, S. Guan, N. Shen, Intermetallics 12 (2004) 1139.
[20] S.J. Pang, T. Zhang, K. Asami, A. Inoue, Mater. Trans. 42 (2001) 376.
[21] S.J. Pang, T. Zhang, K. Asami, A. Inoue, Mater. Trans. 43 (2002) 2137.
[22] Ch. Lou, M. Pan, S. Kou, D. Zhao, W. Wang, Chin. Sci. Bull. 50 (3) (2005) 205–207.
[23] D. Turnbull, Contemp. Phys. 10 (1996) 473.
[24] Z.P. Lu, C.T. Liu, Acta Mater. 50 (2002) 3501.
[25] Z.P. Lu, C.T. Liu, Phys. Rev. Lett. 91 (2003) 115505–115511.
[26] Q.J. Chen, J. Shen, H.B. Fan, J.F. Sun, Y.J. Hugan, D.G. McCartney, Chin. Phys. Lett. 22 (2005) 1736.
[27] X.H. Du, J.C. Huang, C.T. Liu, Z.P. Lu, J. Appl. Phys. 101 (2007) 086108.
[28] A. Morish, PWN Warszawa (1970) 366–367 (in Polish).